Control of Active Multi-Point-Contact Feet for Quadrupedal Locomotion

Alexander Dettmann, Daniel Kühn,
Frank Kirchner

German research center for artificial intelligence
GmbH - Robotics Innovation Center (DFKI RIC)
Bremen, Germany
e-mail: alexander.dettmann@dfki.de

Frank Kirchner
University of Bremen, Faculty of Mathematics and
Computer Science
Bremen, Germany

Abstract — **With increasing sensing, motion, and processing capabilities, robots start to master more and more complex tasks in difficult applications. Especially working in hazardous environments, such as exploring extraterrestrial planets or nuclear disaster sites, demand robotic solutions with advanced locomotion capabilities in unstructured terrain. Four-legged systems can provide the desired mobility. The hominid robot Charlie has, in contrast to most quadrupeds, an active ankle joint with Multi-Contact-Point-Feet to support four-legged as well as two-legged locomotion. In this paper, the advantages of this foot design for four-legged locomotion is analyzed. The paper summarizes briefly Charlie's hardware and software components. In detail, the foot design and the behavior modules which utilize the possibilities of actively controlled Multi-Contact-Point-Feet are described. The experimental results show that a positive effect on traction and range of motion are achieved which improve the mobility of quadrupeds.**

Keywords–quadrupeds; locomotion; foot design; active ankle

I.   INTRODUCTION

In recent years, there has been a growing focus on legged locomotion in robotic systems. The motivation to investigate legged locomotion is due to the possible advantages and versatility of such systems such as: (i) decoupling body orientation from terrain structure, (ii) continuous ground contact path is not needed, (iii) overcoming steep slopes, (iv) numerous ways to apply forces to the environment, (v) handling a wide variety of substrates, (vi) use of limbs as a tool carrier, e.g., for manipulation tasks, (vii) inherent redundancy, and (vii) omnidirectional mobility, among others. Due to these advantages, numerous research groups successfully developed robots that mimic the appearance and/or the locomotion patterns of their natural counterparts.

Multi-legged robots have the intrinsic ability to generate a stable stance with Single-Point-Contact-Feet (SPCF) when using an appropriate walking pattern. These kinds of feet have the advantage to provide traction at any contact angle, e.g., the six-legged robot SpaceClimber [1] is able to overcome rough terrain and sandy slopes of up to ±35°. Also four-legged robots like Starleth [2] or LittleDog [3] showed their cross-country mobility. Humanoid robots such as Atlas [4] or Valkyrie [5] need Multi-Point-Contact Feet (MPCF) to maintain stability on two or even one leg.

Fig. 1 The homid robotic system Charlie

Opposite to most other legged systems, the hominid robot Charlie [6] (Fig. 1) was designed to perform quadrupedal as well as bipedal locomotion similar to their multi-talented biological inspiration, the chimpanzee (*Pan troglodytes*). Due to the desired multi-functionality, and in contrast to other quadrupeds, MPCF with an active ankle joint are used in the rear legs.

Other multi-legged walking robots featuring MPCF like Titan [7] or Roboclimber [8] only come along with passive adaptation mechanisms in the feet to exploit these benefits, which is also true for the foot described in [9]. BISAM [10] is an example where SPCF were replaced by passive MPCF to increase traction.

Since a MPCF on an actuated ankle joint is commonly not used in quadrupeds, we try to answer the question whether it this beneficial for these type of legged systems. Therefore, we first briefly describe the hominid robot Charlie with focus on its foot design (Section II). Then, in Section III, an overview on the behavior-based control structure is given to understand how a foot pitch module can influence the overall walking pattern of a robot. In Section IV, the active MPCF is evaluated and tested during walking. The final section summarizes the results and provides an outlook.

II. Active Multi-Point-Contact Feet

Charlie is a hominid robotic system with 37 active degrees of freedom (DoF) and various proprioceptive and exteroceptive sensors making the robot an ideal test platform to tackle uneven terrain or to master various inclines. Besides the active artificial spine, one unique characteristic is the actively controlled foot design with MPCF, allowing Charlie to walk on four and two legs.

The limb proportions and features like the range of motion (RoM) of chimpanzee legs and feet were analyzed and served as model for the design of the leg structure. Since there is little literature available regarding the documentation of chimpanzee feet, for designing the foot structure the focus was enlarged to all primate feet, including human physiology. The design (Fig. 2) incorporates motors and electronics in the lower leg for realizing a roll and pitch motion, a force-torque sensor, as well as a sole consisting out of passively connected heel, foot arch, ball, and active toes.

The roll and pitch motion is realized by two linear actuators located at the same position like the human calf. The motors are supplemented by reduction gear units and incremental encoders. The relative position is measured by evaluating these encoders while digital Hall sensors are used for motor commutation. A lead screw and spindle nut mechanism is connected to the gear's output shaft. The rotational motion is transmitted via two four-bar spatial linkages to the lower ankle joint segment. The linkages build levers which lengths can be adjusted to produce the required RoM, velocities, or torques. For more details please see [11]. The original passive rotation around the yaw axis was fixed for improved stability.

In [12], Allinger stated that a human foot has a RoM of roll from 10° to -20°, pitch between 20° to -30°, and yaw from 10° to -10°. According to [13], the RoM in apes is slightly larger than in humans, which is why the RoM of the artificial foot is increased compared to the human RoM The maximum joint angles of the ankle joint implemented in Charlie are ranging from -62° up to 69° for the pitch and ±25° for the roll. The maximum angular velocities for both active DoF of an unloaded ankle joint are 130°/s for the pitch and 190°/s for roll motion.

Fig. 2 Lower leg - ankle joint - foot - assembly: Next to the biological inspiration (in the back), the CAD-model (middle) depicts the developed lower leg structure, whereas a photograph of the lower leg and ankle joint with the foot is shown in the front.

To gain an increased perception of the environment, it is necessary to implement multiple sensors and suitable electronics into structures like a foot which is limited in space. Within the rear foot the following sensors are installed: a six-DoF force/torque sensor, an acceleration sensor (three axes), a temperature sensor, and eight absolute encoders (one per toe, one per passive DoF).

In addition, in order to increase the spatial resolution for tactile perception of the environment in a robotic foot, a pressure-sensing array consisting of 49 Force Sensing Resistors (FSR) is installed underneath each rear foot sole. An FSR changes its resistance when a force is applied, so an array can measure the spatial distribution of forces applied to the foot. Size and weight of the selected sensor satisfies structural and electrical requirements. It has a sensing area of 5.1 mm in diameter and a sensitivity of 20 mN/cm^2.

During locomotion, the heel and the ball/toe area are the regions where the main load is applied. Thus, like in human feet, both parts are equipped with a higher sensor density (15 sensors on the heel, eight under each toe) than at the foot arch, which houses twelve sensors (Fig. 3). Additionally, six sensors are placed on the outside of the foot and serve as collision detectors. With this arrangement, a spatial resolution of 0.3 mm^2 to 4.5 mm^2 is achieved.

III. Behavior-Based Motion Control

The reactive motion control is a behavior-based architecture realized in BAGEL [16]. It follows a hierarchical modular concept consisting of general-applicable and robot-specific behavior modules, where every module can contain further submodules to reduce module complexity and to increase module reusability (Fig. 4).

On the highest control layer, a Central Pattern Generator (CPG) behavior module is used to derive a gait-dependent step cycle for every limb and for the body. This signal is sent to every leg or arm controller in which a state pattern generator is triggered to derive a foot trajectory. The trajectory is then superposed by outputs of other behavior modules such as the basic position defined by the desired robot posture.

All posture and locomotion parameters are defined in an ideal frame which is parallel to the ground, the so called locomotion frame (*Loco Frame*). The generated feet positions are transformed from *Loco Frame* to the robot coordinate system (*Robot Frame*) which is fixed to the robot. With the help of the body forward kinematics, a target
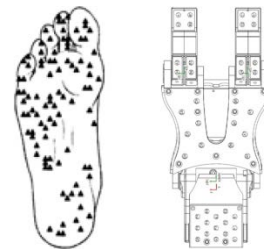

Fig. 3 (l.) Schematic drawing of the distribution of mechanoreceptors in the human foot (image adapted from [14]) and (r.) schematic drawing of the MPCF. Each circle indicates the position of a FSR sensor.
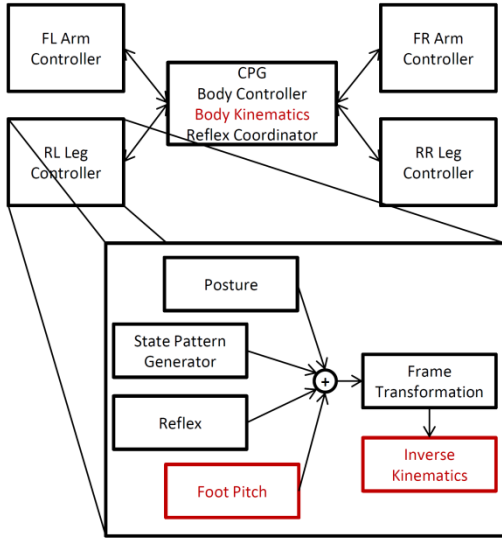
Fig. 4 Behavior-based control architecture. Black boxes represent general behavior modules used in several robots. The red boxes represent behavior modules which utilize the specific characteristicsa of Charlie's morphology

position for each foot in its limb coordinate system (*LimbBase_e Frame*) is calculated. Finally, inverse kinematics are used to compute the joint targets.

A. Posture

The basic stance is defined by the *step_base_{x,y}* parameter and an additional *arm_offset_y* to define foot positions well suited for both, leg and arm kinematics (Fig. 5). It is also possible to set an individual offset for each limb. The transformation from *Loco Frame* to *Robot Frame* is realized by setting a desired *body_shift_{x,y,z}* and *body_rot_{roll,pitch,yaw}*.

In general, all parameters can be changed during runtime. Only parameters, which influence the basic stance are set when the corresponding leg is in the air to avoid shear forces as well as tension between the limbs.

B. Central Pattern Generator

The CPG module generates an internal clock, which triggers different phases of a walking cycle. It consists of a period generator, a period coordinator, and a gait generator. This period generator generates a periodic, normalized, saw-like curve from zero to one representing the internal robot clock. The time step increment (t_{step}) depends on the desired step cycle time (t_{cycle}) and the update rate of the control (t_{period}) (1).

$$t_{step} = \frac{t_{period}}{t_{cycle}} \qquad (1)$$

The period coordinator starts and stops the internal clock depending whether a movement is desired or not. When movement is not any longer desired, no further leg is allowed to start the lifting movement. However, the step cycle continuous (period counter will increase) until all legs (which were in swing phase when the motion stop command was triggered) are placed on the ground. If a robot movement is again desired, the walking cycle will be continued with the next leg originally scheduled for liftoff, before it was interrupted.
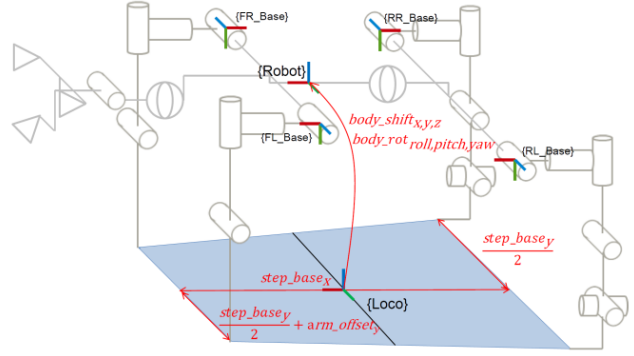

Fig. 5 Charlie's kinematics, frames and parameters to define the posture

The gait generator defines at what time each leg starts with their movement. It supports walking gaits for two-legged and four-legged posture. The parameter *phase_shift* can be set to influence the time between diagonal legs. A full phase shift will evenly distribute the start of each leg movement, whereas no phase shift will lead to a trot gait in the case of four-legged walking (Fig. 6).

C. Body Controller

This behavior module shifts the body over the ideal CoSP in order to maintain a stable walking posture. With the knowledge of the gait, it knows which legs to use for computing the CoSP (2).

$$CoSP = \frac{\sum_{e=1}^{E} foot\_pos_e}{E} \qquad (2)$$

, where E is the number of legs in stance phase and foot_pos_e their desired position in *Loco Frame*.

A spline interpolator is used to generate a curve for every swing time of a leg, having its mid target over a scaled CoSP and the target in the middle of the current and consecutive CoSP. For the target point, a target speed is estimated to avoid a start-stop behavior during leg transition. Thus, for four-legged walking, an eight-shaped trajectory is generated.
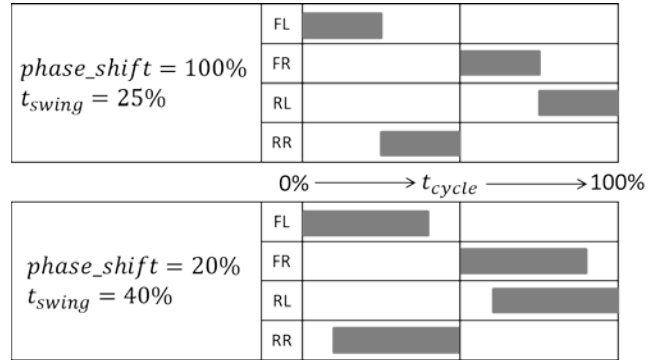

Fig. 6 Gait graphs for different CPG parameterizations resulting in walk (top) and trot (bottom)

Constantly, the Zero Moment Point (ZMP) [15] is calculated and transformed into Loco Frame. While walking on plane ground, it will follow the desired body movement. But as soon as the robot gets tilted, e.g., when climbing over obstacles or entering a slope, a difference will occur. The body controller compensates this difference by preventing the ZMP to cross one edge of the support polygon and thus maintaining a stable walking behavior.

D. Limb Controller

This behavior module generates a Cartesian foot trajectory, based on the current progress of the step cycle. A step cycle consists of a stance (t_{stance}) and a swing phase (t_{swing}), see Fig. 7. The latter is divided into a lift (t_{lift}), shift (t_{shift}), and down phase (t_{down}), each defined by a portion of the overall step cycle (3). In order to realize a statically stable walking pattern, their sum, i.e. the swing time, shall not exceed a maximum leg time, defined by the gait.

$$1 = t_{stance} + t_{swing} = t_{swing} + t_{lift} + t_{shift} + t_{down} \quad (3)$$

A leg can only enter the lift phase when movement is desired. During stance, a leg is moved on the ground with a speed defined by the length of each step in longitudinal and lateral direction ($step\_length_{x,y}$) and the step cycle time, thus defining the overall robot speed (4).

$$v_{xy} = \frac{step\_length_{xy}}{t_{cycle}} \quad (4)$$

Each phase has its target point which is reached within its given target time either using a linear or spline interpolator. The linear interpolator is used for the stance phase as well as for the horizontal components in the lift and down phase to ensure no upcoming shear forces due to different speeds. The lift stops and the down phase starts at the full step height ($step\_length_z$). During these phases the leg is moved against the direction of movement to compensate it. Consequently, a vertical lift with respect to the environment is realized, which is beneficial while climbing over obstacles.

Since the generated trajectory requires much movement range, one can increase the parameter *phase_shortage* to reduce the lift and down phase as well as their target values and resulting in a smooth curve with a prolonged shift phase. Consequently, less movement range is required, which enables larger and faster steps (red curve).

When traversing unstructured terrain, the generated trajectory needs be adapted. Compared to walking on flat terrain, two situations may occur. First, the leg needs to crouch when contact was detected with the foot sensors during down phase. To prevent tipping over, the z-position of the foot has to stay constant, so a compensating offset is generated which superposes the normal walking trajectory. Second, the leg must stretch when no contact is established during stance phase, e.g. stepping in a hole.

Since the local elevation and depression reflex cannot take the state of the entire robot into consideration, blind reaction movements might lead to instability. Therefore, a reflex coordinator can influence a leg's reflex behavior for two reasons: (i) inhibiting stretching a leg when the robot is tilted in opposite direction as well as inhibiting crouching
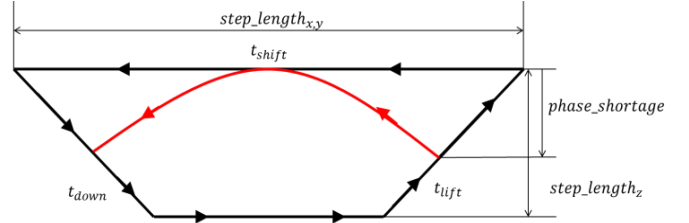

Fig. 7 Foot trajectory and its configuration parameters. The red curve shows the generated trajectory for phase_shortage of 0.5

when the robot is tilted in the same direction of the leg and (ii) reducing all reflex outputs when either all legs in stance phase are stretched or crouched.

E. Ankle Controller

Charlie's foot itself is a complex system consisting of a sole with many pressure sensors, an active roll-pitch ankle joint, a force torque sensor, and a micro controller. This gives the possibility to implement a local controller that uses the measured Center of Pressure (CoP) to directly add local offsets to the desired roll and pitch angles. Thus, surface irregularities can directly be compensated without the need of a high-level control. To realize the desired behavior, a spring-damper behavior is implemented, which adapts its stiffness with respect to the step cycle. During down-phase, the foot is soft in order to adapt to the ground. During progress of the stance-phase, the achieved offset is kept, but the stiffness is increased so that the corresponding leg can support the forward motion. Though this behavior is desired for quadrupedal walking, its parameterization is context-dependent, e.g. going uphill or downhill. A complete different context would be bipedal walking. Here, the ankle needs to stabilize the feet. This is realized by acting against the incoming forces. Due to the context-dependent required functionality, the local controller module can be adapted by higher layers. The specific implementation details can be found in [17].

In addition, the ankle can be pitched actively by the foot pitch behavior module. The gait-dependent foot pitch modulation can be varied according the needs of each phase of the step cycle (Fig. 8). Thus, the heel can be lifted just before the lift phase starts to allow larger steps. During shift phase, the toes can be lifted to reduce the chance of hitting an obstacle unintendedly with the toes first. It also possible to walk entirely on the ball of the foot. In order to maintain the position of the ball, the resulting difference of the ankle position is added before calculating the inverse kinematics of the leg. Thus, no shear forces are produced when the ankle is pitched.
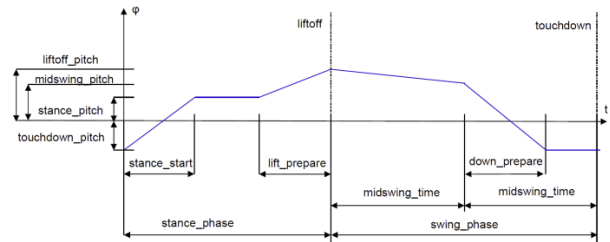

Fig. 8 Ankle pitch cycle and its parameters

IV. EXPERIMENTAL EVALUATION

In this section, the results of an experimental evaluation of the active ankle with MPCF are shown. First, the traction of the presented MPCF is compared to a representative SPCF. Second, the correctness of the integrated FSR array is checked. Third, the integration of the state-dependent foot pitch within a walking pattern is analyzed concerning the RoM. Finally, the influence of the ground adaptation capability realized by the local ankle controller is evaluated on different slopes.

A. Foot Traction

The static friction of a spherically shaped foot, here the one used by the SpaceClimber robot [1], was compared with the feet developed for the hominid robot Charlie (Fig. 9). Each foot was mounted to a vertical linear guide and loaded with different weights from 2 kg to 8 kg as normal force. The feet were placed on a rollable plate, which was covered with sandpaper of two different grain sizes (360 and 1500). This plate was horizontally pulled away at different angles (0°, 45°, 90°, 135°, and 180°). An angle of 0° corresponds to pulling the base plate forward, 180° implies pulling the plate in heel direction. All measurements for the spherically shaped and the rear foot were repeated five times. The average maximum recorded force, i.e. the frictional force F_R was used for further processing.

To evaluate the results, regardless of the applied loads, the friction coefficient μ ($\mu = F_R/F_N$) is calculated for the above mentioned five directions. As shown in Fig. 9, the friction coefficient of the rear foot exceeds the one of the spherical shaped foot in all directions and on both surfaces except for the finer grain size while pulling at a 90° angle. In this direction, the spherical shaped foot has a higher friction coefficient of about 3.6%.

Striking is the asymmetry of the friction values of the developed foot. While walking, the main load direction occurs at 0° and 180°. For this direction, the friction coefficient is higher than compared to the lateral load directions. This asymmetry is mainly caused by the passive adaptation capabilities implemented in the foot, which only have an effect on longitudinal forces.
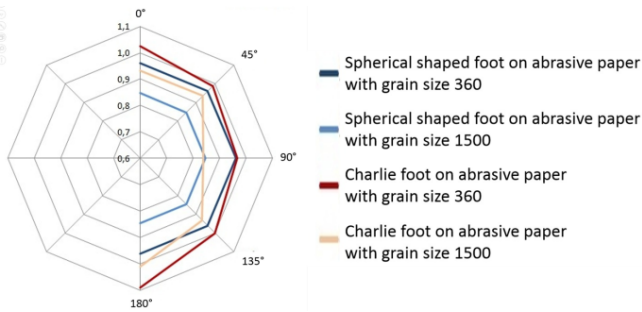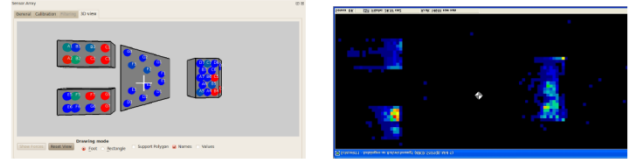

Fig. 9 Friction coefficient measurement of spherically shaped feet and the developed MPCF foot

(a) Visualization of the incoming sensor array data in a quadrupedal pose.
(b) Visualization of applied forces on the Tekscan force plate.

Fig. 10 Locally preprocessed sensor array data compared to externally measured data on a force plate

B. FSR Sensor Array

In order to examine the output of the sensor array for its correctness, Charlie is placed with one rear foot on an industrial tactile pressure and force measurement plate designed by Tekscan[1].

Fig. 10 shows simultaneously recorded screenshots of the graphical user interface used to visualize Charlie's sensor array data (Fig. 10(a)) and the one from the Tekscan software (Fig. 10(b)). For Charlie's sensor array, blue means that no pressure is applied, green indicates a medium pressure, and red a high pressure. The same color coding can be seen in the Tekscan software, except that the color blue indicates a slight pressure. The white cross in Fig. 10(a) and the silvery square in Fig. 10(b) indicate the local CoP Please note that due to a higher measurement range of each taxel of the Tekscan force plate, the color coding is not comparable. Nevertheless, by comparing the recorded data and the resulting pictures, it can be clearly seen that a mapping of the pressure points as well as a local CoP calculation can be achieved in appropriate accuracy within the sensory foot.

C. Range of Motion Analysis

As described in Section III, Charlie's control is based on several behavior producing modules which all contribute to the overall locomotion behavior. Due to the hierarchical structure, a set of basic behavior modules can be used to generate locomotion patterns for every type of four-legged system. In addition, the foot pitch module modulates the default trajectory by utilizing the special kinematical structure of Charlie. Here, the benefit of this module concerning the RoM is investigated. Therefore, the same walking pattern was used with and without activated gait-dependent foot pitch module (Table I).

Table I Walking parameters during ROM analysis

$step\_base_x$	0.6 m	t_{cycle}	6 s
$step\_base_y$	0.28 m	t_{lift}	7%
$body\_shift_x$	0.05 m	t_{shift}	8%
$body\_shift_z$	0.5 m	t_{down}	8%
$body\_rot_{pitch}$	-5°	$phase\_shortage$	0.5
$COSP\_scale$	50%	$phase\_shift$	100%
$step\_length_x$	0.36 m	$foot\_pitch/liftoff\_angle$	30°
$step\_length_z$	0.5 m	$foot\_pitch/lift\_prepare$	20%

---

[1] https://www.tekscan.com/products-solutions/systems/i-scan-system?tab=sensors accessed Feb. 2016

During walking, the first hip joint and the knee joint contribute most to the forward motion. When taking a look on the required joint angles and velocities (Fig. 11), one notices that the demands on movement range and velocity are reduced, when walking is supported by the foot pitch behavior. Especially in the phase around liftoff (from 75% up to 8%) the usage of the foot pitch compensates the stretching of the leg, resulting in a more bent knee. This has the major advantage that more movement range of the leg remains, which is crucial when reactive behaviors want to modulate the desired foot position, e.g., stretching the leg further when the foot steps into a hole.

Ina addition, the maximum longitudinal step length was evaluated by increasing $step\_length_x$ until a leg loses ground contact before the actual lift phase starts, signalizing that the maximum RoM was exceeded. Without using the foot pitch behavior, a maximum step length of 390 mm can be achieved. Using a 30° liftoff pitch angle increases the maximum step length to 470 mm, which corresponds to a gain of 20%.
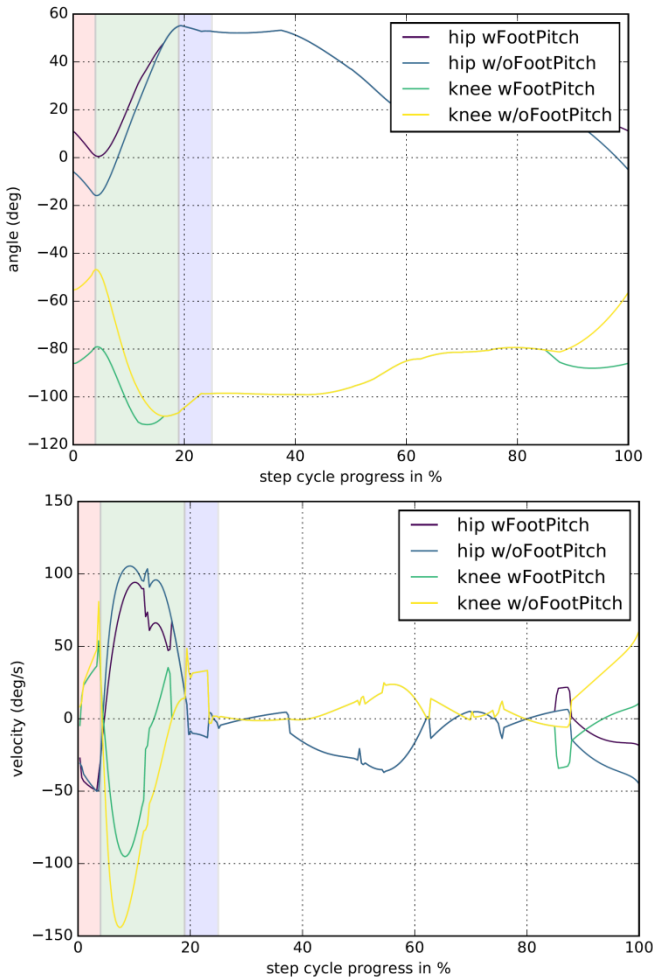

Fig. 11 Required joint angles and velocities during walking at constant speed (60 mm/s) with and without utilization of the foot pitch behavior. Lift shift and down phase is colored with red, green, and blue background, respectively

Regarding the required velocities, the active usage of the foot pitch has a higher influence on the knee joint than on the hip joint. The knee joint velocity during lift phase is almost halved. Thus, Charlie is capable of moving faster with activated foot pitch module.

D. Stability in Inclines

In [6], it was shown that the power consumption with activated local ankle control is slightly less for going uphill and more when walking downhill. In this experiment, the influence of the local ankle control on the stability in inclines was evaluated. For this experiment, an in infinitely variable, indoor ramp with a wooden surface was used (Fig. 12). The incline is increased in 5° steps and ranges from -20° to 20°. A positive degree indicates uphill walking and a negative degree stands for downhill walking. The walking pattern was adjusted compared to the previous experiment. In order to increase the traction, the walking speed was reduced to 30 mm/s and the gait-dependent foot pitch was deactivated.

Fig. 13 and Fig. 14 show the robot's average ZMP shifting during one step as top view. This way, the ZMP movement and its deviation (visualized by gray bars) from the mean value can be seen on the x-axis and y-axis. The progress of the walking cycle is indicated by the changing color from green to blue. For a better overview, additional numbers are attached to the respective curve.

By comparing the movement of the ZMP in an incline of 20°, it can be seen that the deviation is reduced witch activated local control loop. This is the result of the reduction of occurring torques in the beginning of the stance-phase. In addition, a better form closure between sole and ground is achieved with active local control loop, which leads to an increased traction.

This is similar to the result in [6] regarding the ZMP motion in the gravel field, where the local control loop also produced a motion with less deviation, resulting in a more reliable walking. A smaller deviation can be seen in all experiments, where the robot is walking uphill. While walking downhill with activated local controller, the deviation of the ZMP is much smaller than for uphill walking. Still, it shows an improvement for all inclines up to -10°. However, in slopes with an incline of -15° or -20°, the mean deviation is equal or even larger with activated control loop (Fig. 14).
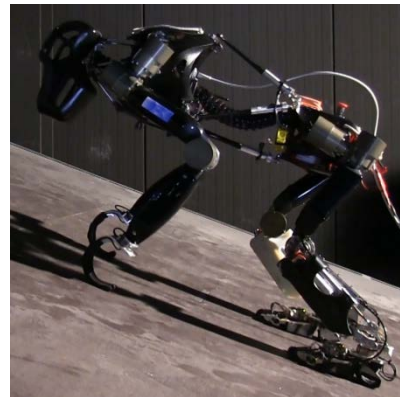

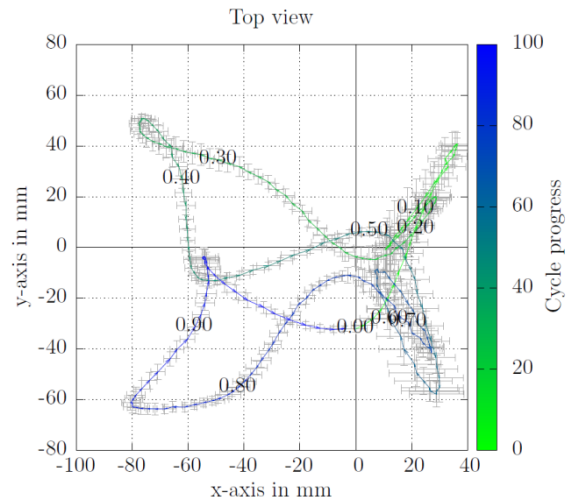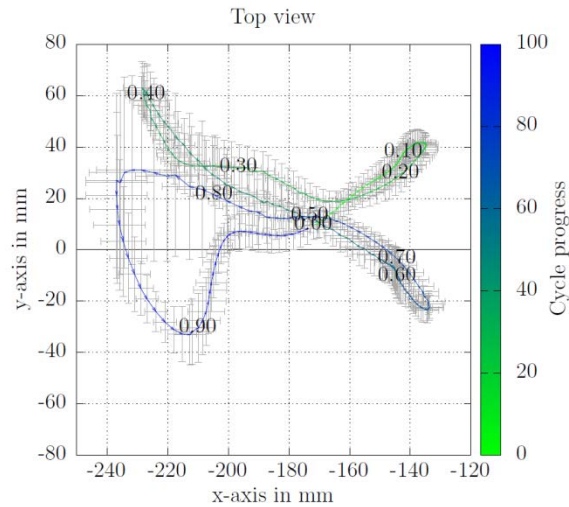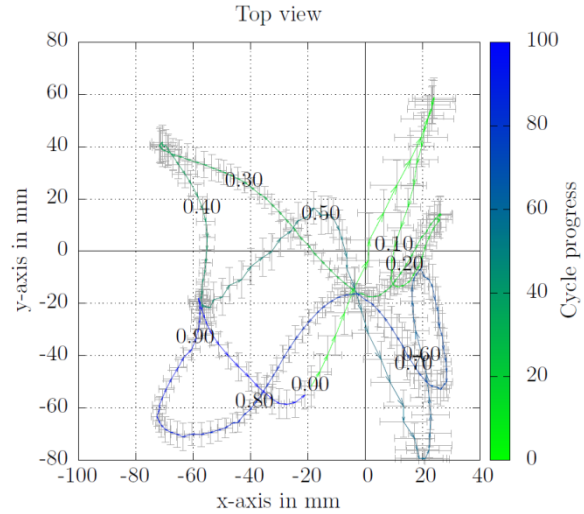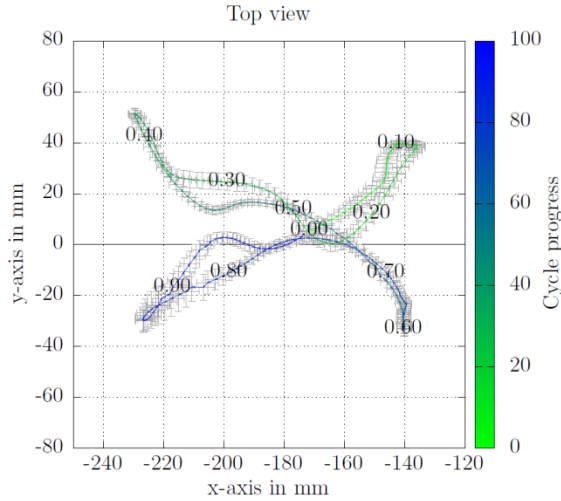Fig. 12 Charlie walking uphill a 20° incline

Fig. 13 ZMP while walking uphill a slope of 20° with (bottom) and without (top) local ankle controller [18]

Fig. 14 ZMP while walking downhill a slope of -20° with (bottom) and without (top) local ankle controller [18]

In positive inclines as well as in slopes with inclines of up to -10° the robot's CoM moves in a more consistent manner with only a few outliers when the local control loop is active. The shown ZMP trajectories are more erratic compared to CoM trajectories, because of occurring short-term accelerations during walking and autonomous posture changes, but allow a clearer presentation of the differences between activated and deactivated local control loop. Yet, also for the ZMP trajectories, a smaller deviation is observed in all uphill walking scenarios as well as in downhill walking up to -10°. Lower outliers indicate a more stable behavior of the robot.

For this experiment, the central question is whether the stability is sufficiently increased to justify the increased energy consumption. Unfortunately, for inclines of more than -10°, a larger deviation is observed in the ZMP trajectory. It can be stated that the robot's increased energy consumption does not result in a more stable downhill walking.

V. CONCLUSION AND OUTLOOK

In this paper, an actively controlled ankle joint with MPCF was presented. The design incorporates a roll and pitch DoF as well as pressure and force-torques sensors and a microcontroller for local preprocessing. The active MPCF are integrated in the rear legs of a hominid robot. The utilization of such a foot design was integrated within a behavior-based control scheme in two ways. First, a local controller was added that realizes adaptation capabilities towards unstructured terrain. Second, a gait-dependent foot pitch behavior was introduced to support the walking.

Through an experimental evaluation, it was shown, that the foot design improves traction in longitudinal direction. In addition, the pressure sensors underneath the sole allow a precise estimation of the force distribution within the MPCF. The proprioceptive data is used to locally adapt towards obstacles. It was shown that the foot adaptation leads to a larger contact area providing more traction. In addition less ground forces are applied leading to smoother locomotion. This is especially true for walking uphill whereas descending

steep declines is more instable. One possible solution to remedy the situation is a context-based adaption of the local control loop parameters. It was also shown that the active integration of the foot pitch to lift the heel before lifting the complete leg has a positive influence on the RoM. In addition, the demands on joint angles and velocities can be reduced.

Though, the increase in structural and algorithmic complexity has to be faced, the mentioned advantages lead to the conclusion that actively controlled MPCF can increase the mobility of quadrupeds. In near future, the proposed behavior modules will be tested in combination with other reactive behaviors to overcome challenging obstacles fast and reliably. In addition, the large amount of possibilities to control the robot, i.e. parameters to generate different walking patterns, need to get adapted autonomously with respect to the given task as well as the current state of the environmental and the robot itself.

REFERENCES

[1] S. Bartsch, T. Birnschein, M. Römmermann, J. Hilljegerdes, D. Kuehn, and F. Kirchner, "Development of the six-legged walking and climbing robot spaceclimber," Journal of Field Robotics, vol. 29, 2012.

[2] M. Hutter, C. Gehring, M. Bloesch, M. A. Hoepflinger, C. D. Remy, and R. Siegwart, "Starleth: A compliant quadrupedal robot for fast, efficient, and versatile locomotion," in Climbing and Walking Robots (CLAWAR), 2012.

[3] M. P. Murphy, A. Saunders, C. Moreira, A. A. Rizzi, and M. Raibert, "The littledog robot," The International Journal of Robotics Research, vol. 30, no. 2, pp. 145–149, 2011. [Online]. Available: http://ijr.sagepub.com/content/30/2/145.abstract

[4] M. Fallon, S. Kuindersma, S. Karumanchi, M. Antone, T. Schneider, H. Dai, C. P. D'Arpino, R. Deits, M. DiCicco, D. Fourie, T. Koolen, P. Marion, M. Posa, A. Valenzuela, K. Yu, J. Shah, K. Iagnemma, R. Tedrake, and S. Teller., "An architecture for online affordancebased perception and whole-body planning," MIT CSAIL, Tech. Rep., 2014.

[5] N. A. Radford, P. Strawser, K. Hambuchen, J. S. Mehling, W. K. Verdeyen, A. S. Donnan, J. Holley, J. Sanchez, V. Nguyen, L. Bridgwater, et al., "Valkyrie: Nasa's first bipedal humanoid robot," Journal of Field Robotics, vol. 32, no. 3, pp. 397–419, 2015.

[6] D. Kuehn, M. Schilling, T. Stark, M. Zenzes, and F. Kirchner, "System design and field testing of the hominid robot charlie," Journal of Field Robotics, 07 2016.

[7] S. Hirose, K. Yoneda, and H. Tsukagoshi, "Titan vii: Quadruped walking and manipulating robot on a steep slope," in Proceedings of the 1997 IEEE International Conference on Robotics and Automation, Albuquerque, New Mexico, 1997. [Online]. Available: http://ieeexplore.ieee.org/stamp/stamp.jsp?arnumber=00620085

[8] G. Acaccia, L. Bruzzone, R. Michelini, R. Molfino, and R. Razzoli, "A tethered climbing robot for firming up high-steepness rocky walls," in Proc. of the 6th IAS Intl. Conf. on Intelligent Autonomous Systems, 2000.

[9] K. Tokuda, T. Toda, Y. Koji, M. Konyo, S. Tadokoro, and P. Alain, "Estimation of fragile ground by foot pressure sensor of legged robot," in IEEE/ASME International Conference on Advanced Intelligent Mechatronics (AIM 2003), 2003, pp. 447 – 453.

[10] J. Albiez, R. Dillmann, and T. Hinckel, "Reactive foot-control for quadruped walking," in 3rd International Symposium on Adaptive Motion in Animals and Machines, 2005.

[11] K. Fondahl, D. Kuehn, F. Beinersdorf, F. Bernhard, F. Grimminger, M. Schilling, T. Stark, and F. Kirchner, "An adaptive sensor foot for a bipedal and quadrupedal robot," in Proceedings of IEEE International Conference on Biomedical Robotics and Biomechatronics, 2012.

[12] T. L. Allinger and J. R. Engsberg, "A method to determine the range of motion of the ankle joint complex, in vivo," Journal of Biomechanics, vol. 26, no. 1, pp. 69 – 76, 1993. [Online]. Available: http://www.sciencedirect.com/science/article/pii/002192909390614K

[13] J. M. DeSilva, "Functional morphology of the ankle and the likelihood of climbing in early hominins," Proceedings of the National Academy of Sciences, vol. 106, no. 16, pp. 6567–6572, 2009. [Online] Available: http://www.pnas.org/content/106/16/6567.abstract

[14] P. M. Kennedy and J. T. Inglis. Distribution and behaviour of glabrous cutaneous receptors in the human foot sole. The Journal of Physiology, 538(Pt 3):995 - 1002, 2002.

[15] M. Vukobratovic and B. Borovac. Zero-moment point - thirty five years of its life. I. J. Humanoid Robotics, 1(1):157-173, 2004.

[16] M. Langosz, L. Quack, A. Dettmann, S. Bartsch, and F. Kirchner, "A behavior-based library for locomotion control of kinematically complex robots," Int. Conf. on Climbing and Walking Robots, 2013

[17] D. Kuehn, F. Bernhard, A. Burchardt, M. Schilling, T. Stark, M. Zenzes, and F. Kirchner. (2014). Distributed computation in a quadrupedal robotic system. International Journal of Advanced Robotic Systems, 11.

[18] D. Kuehn, Design and development of a hominid robot with local control in its adaptable feet to enhance locomotion capabilities. 2016, Dissertation